Journal of Materials Chemistry A

COMMUNICATION

View Article Online
View Journal | View Issue

Cite this: J. Mater. Chem. A, 2019, 7, 22898

Received 17th September 2019
Accepted 25th September 2019

DOI: 10.1039/c9ta10269h

rsc.li/materials-a

Probing into the origin of an electronic conductivity surge in a garnet solid-state electrolyte†

Yongli Song,‡[a] Luyi Yang,‡[a] Lei Tao,[b] Qinghe Zhao,[a] Zijian Wang,[a] Yanhui Cui,[a] Hao Liu,[a] Yuan Lin[ac] and Feng Pan*[a]

Herein, through studying the electronic conductivity of a garnet electrolyte $Li_7La_{2.75}Ca_{0.25}Zr_{1.75}Nb_{0.25}O_{12}$ (LLCZN) at different temperatures, a model to describe the electron transfer process within garnet electrolytes is proposed for the first time. In this model, electronic conductivity is mainly determined by the barrier height and bias between the grain boundaries of LLCZN. As the external voltage polarization increases with ion current densities and finally exceeds a threshold value, electron conductivity concentration at grain boundaries increases sharply to the critical point for the combination between Li-ions and electrons. Lithium metal will consequently deposit on the grain boundaries and short circuit LLCZN. According to the results, lowering the voltage polarization across the solid electrolyte and increasing the electron transfer energy barrier at grain boundaries are two effective approaches to realize practical applications of garnet electrolytes in solid-state lithium metal batteries.

Introduction

Solid electrolytes (SEs) are considered as a critical roadmap for Li metal batteries with advantageous energy density. Among various SSE materials, garnet-type oxides, $Li_7La_3Zr_2O_{12}$ (LLZO) in particular, are considered promising because of their high ionic conductivity, good electrochemical stability and high chemical stability against Li metal. However, the application of LLZO in Li metal batteries suffers from high LLZO/Li interfacial resistance and Li dendrite growth in LLZO.[1] Previous results have shown that LLZO generally suffers from low critical current density (CCD), above which Li dendrites form rapidly and a short circuit occurs abruptly.[2] Since Li dendrites tend to propagate along the grain boundaries and voids in LLZO,[2] many factors including relative density,[3,4] lithium ion diffusivity,[5,6] pre-existing defects in the surface and bulk,[7] inhomogeneous lithium plating due to insufficient LLZO/Li interfacial contact[2,8–10] and temperature[9,11] are reported to be related to Li dendrite growth. Recent studies have shown that the relatively high electronic conductivity should be responsible for Li dendrite formation in LLZO.[12–14] In our previous work, it was proposed that Li^0 is formed at the grain boundary of a garnet electrolyte due to the combination of Li^+ and electrons.[15] Generally speaking, the electronic conductivity of semiconductors increases with temperature. Therefore, if the short circuit process is simply dependent on the electronic conductivity, a lower CCD is expected at elevated temperature. However, the experimental results have shown otherwise,[9] indicating that more factors should be taken into consideration. To date, a model has yet to be established to describe the electron conduction and Li dendrite formation in garnet-type electrolytes.

Herein, a new model is proposed to investigate the short-circuit mechanism of a garnet-type solid electrolyte $Li_7La_{2.75}Ca_{0.25}Zr_{1.75}Nb_{0.25}O_{12}$ (LLCZN), where Ca^{2+} and Nb^{5+} are doped into LLZO for achieving a lower sintering temperature, stable cubic garnet phase and higher ionic conductivity.[16,17] In this model, a high external voltage applied across the solid electrolyte could cause the energy barrier breakdown of the grain boundaries. As a result, the electronic conductivity of LLCZN dramatically increases, therefore leading to the short circuit of the SSE.

Results and discussion

The XRD pattern (Fig. S1a†) of LLCZN can be well indexed to the reference pattern of standard $Li_5La_3Nb_2O_{12}$ with a cubic garnet phase (PDF 80-0457). The cross-section SEM images of LLCZN pellets are shown in Fig. S1b,† indicating that densely sintered LLCZN electrolyte was obtained. The ionic conductivity of the

[a]School of Advanced Materials, Peking University Shenzhen Graduate School, Shenzhen 518055, China. E-mail: panfeng@pkusz.edu.cn

[b]Laboratory for Space Environment and Physical Sciences, Harbin Institute of Technology, Harbin 150001, People's Republic of China

[c]Institute of Chemistry, Chinese Academy of Science, Beijing 100080, People's Republic of China

† Electronic supplementary information (ESI) available. See DOI: 10.1039/c9ta10269h

‡ These authors contributed equally to this work.

LLCZN polycrystalline electrolyte is measured and calculated from the electrochemical impedance spectra (EIS) shown in Fig. S1c.† As a result, the ionic conductivity of LLCZN (1.2×10^{-4} S cm^{-1} at 25 °C) is in line with literature values for garnet electrolytes.[18]

Origin of an electronic conductivity surge

First, the electronic conductivity of LLCZN was measured in a Li/LLCZN/Au cell. As shown in Fig. 1a, by applying a constant voltage (ΔE) *versus* the open circuit potential (OCP), a steady-state current (I_{ss}) can be obtained. Then the electronic conductivity (σ_e) can be calculated.[10] At 1.3 V, the electronic conductivity of LLCZN at 25 °C is calculated to be 2.53×10^{-8} S cm^{-1}.In addition, the value of σ_e increases with temperature, which agrees with the previous report.[12] By plotting I_{ss} *versus* ΔE, it can be seen from Fig. 1b that at a lower voltage range, the value of I_{ss} increases slowly, indicating a constant electronic conductivity. As higher voltages are applied, the exponential increase of I_{ss} eventually becomes non-linear, which implies increasing electronic conductivities. The relationship between bias voltage and electronic current is investigated by simulation as shown in Fig. S2,† where *I–V* curves can be well fitted using the following equation where electronic current density of varistors increases exponentially with biased voltage:[19]

$$I = I_0 (-q\phi/k_B T)[1 - \exp(-q\Delta E/pk_B T)] \quad (1)$$

where I_0 is a temperature-related constant, q is the elementary charge, ϕ is the grain boundary barrier, k_B is the Boltzmann constant, T is the temperature and p is the number of barriers per unit of length of the polycrystalline. Here, the voltage corresponding to the turning point of electronic conductivity is defined as the threshold voltage (V_T), which gradually decreases as the temperature increases (2.10 V at 25 °C, 2.03 V at 40 °C, 1.92 V at 50 °C and 1.85 V at 60 °C). Similar to varistors such as TiO_2 and SnO_2, electric breakdown could occur at grain boundaries of LLCZN as the external electric field exceeds V_T,[20,21] leading to a sharp increase of electronic conductivity. In addition, as shown in Fig. 1c, the *I–V* curves of two LLCZN pellets with different thicknesses are measured. By normalizing the thickness (inset), the *I–V* characteristic curves are almost the same, indicating that the V_T values are dictated by LLCZN grain boundaries so that the influence of the electrode/electrolyte interface can be excluded.[22] As presented in Fig. 1d, when ΔE = 2.1 V, the total impedance of LLCZN becomes significantly larger compared to that under OCP (shown in Fig. S3†), indicating that the ionic conductivity can be negligible due to the depletion of Li-ions at the Au working electrode, and the total impedance only represents electronic resistance. As ΔE further increases to 2.5 V, the impedance decreases, indicating a higher electronic conductivity. The values of total conductivity calculated from EIS (2.18×10^{-6} S cm^{-1} at 2.1 V and 3.41×10^{-6} S cm^{-1} at 2.5 V) are consistent with those calculated from the potentiostatic results in Fig. 1b (2.08×10^{-6} S cm^{-1} at 2.1 V and 3.14×10^{-6} S cm^{-1} at 2.5 V), further confirming that the EIS only exhibit the electronic resistivity of LLCZN. The impedance spectra are well fitted using an equivalent circuit with two overlapping semi-circles: the small one at high frequencies can be assigned to electron-transfer impedance in the bulk of LLCZN (R_{eB}, C_{eB}) whereas the large one at low frequencies can be assigned to that of the grain boundary (R_{eGB}, C_{eGB}).[23,24] It is worth noting that the impedance in the bulk barely changed with external voltage while the grain boundary impedance decreases sharply with voltage, further confirming that it is the electric breakdown at grain boundaries that causes the electronic conductivity surge in LLCZN.

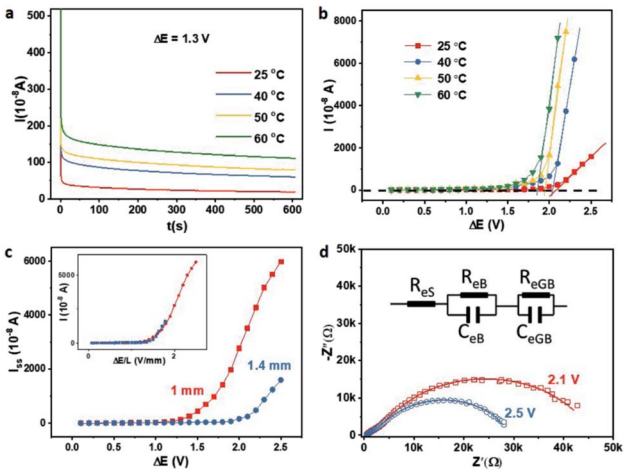

Fig. 1 (a) Chronoamperometry results of an Au/LLCZN/Li cell at different temperatures with an applied voltage of 1.3 V; *I–V* curves of the Au/LLCZN/Li cell (b) at different temperatures and (c) using LLCZN pellets with different thicknesses; (d) impedance spectra of the Au/LLCZN/Li cell under various external voltages.

V_T *vs.* short circuit voltage (V_{sc})

The CCDs of LLCZN at various temperatures were then invested by performing galvanostatic cycling for Li/LLCZN/Li symmetric cells with increasing current density of 0.1 mA cm^{-2} per step. It is noteworthy that in order to exclude the influence of Li/LLCZN for all measurements, a minimum amount (3 μL) of liquid electrolyte was added between Li and LLCZN in order to create a fully wetted Li/LLCZN interface and avoid inhomogeneous lithium plating.[15] From the potential profile of the cell in Fig. 2a, it can be seen that LLCZN exhibited stable Li plating and stripping processes at current densities lower than 0.4 mA cm^{-2}. At 0.4 mA cm^{-2}, an abrupt voltage drop occurs showing that the cell is short-circuited at this current density. Therefore, the CCD of LLCZN is determined to be 0.4 mA cm^{-2} under these testing conditions. It is also noteworthy that the value of CCD represents a narrow range of current densities. As presented in Fig. S4,† when the current density is 0.35 mA cm^{-2}, the cell can be cycled for 100 h without a short circuit. However, as the current density gradually increases from 0.38 mA cm^{-2} to 0.41 mA cm^{-2}, the cycling time before the short circuit dramatically decreases from 30 h to 0.04 h, indicating that the phenomenon of CCD becomes prominent around 0.4 mA cm^{-2}. The CCDs of LLCZN at 40 °C, 50 °C and 60 °C were measured to be 0.6 mA cm^{-2}, 0.7 mA cm^{-2} and 0.9 mA cm^{-2}, respectively (see Fig. 2b–

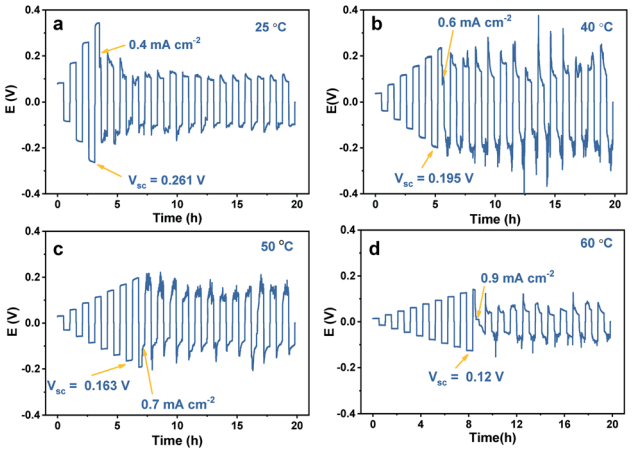

Fig. 2 Lithium plating/stripping performance of Li/LLCZN/Li symmetric cells at various temperatures under step-up current densities with 0.1 mA cm^{-2} per step.

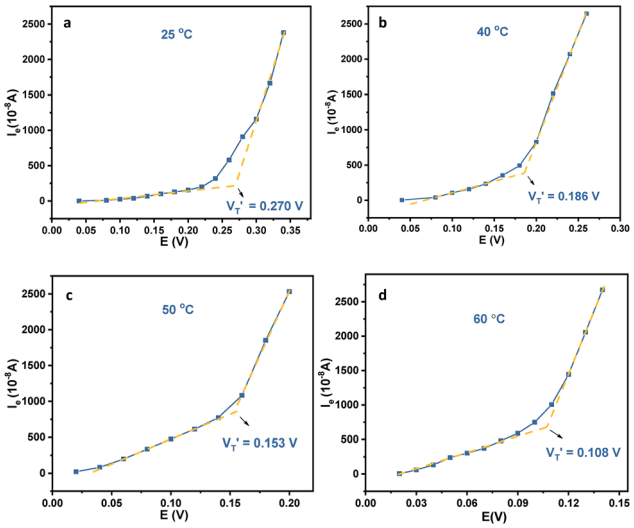

Fig. 3 Calculated *I*–*V* curves of the Li/LLCZN/Li cell at various temperatures.

d). The highest corresponding voltages obtained before the short circuit (V_{sc}) show an opposite tendency. V_{sc} is measured to be 0.26 V, 0.19 V, 0.16 V and 0.12 V at 25 °C, 40 °C, 50 °C and 60 °C, respectively, which has the same tendency of V_T.

As discussed above, correlations are expected to exist between V_T and V_{sc} because electronic conductivity is found to be the main cause for the short circuit of garnet electrolytes.[12,15] Although they both decrease with temperature, their values are significantly different, which might be due to the different cell configurations: V_T and V_{sc} are measured in Au/LLCZN/Li and Li/LLCZN/Li cells, respectively. However, the estimation of electronic conductivity is not experimentally applicable in a Li/LLCZN/Li cell since Li-ions will serve as charge carriers and the ionic conductivity of SSEs is generally hundreds or thousands of times higher than their electronic conductivity.

The effect of Li^+ conduction on electronic conductivity

In order to decouple electronic conductivity in Li/LLCZN/Li cells, an alternative strategy was proposed to indirectly estimate the value of electronic current. The EIS of Li/LLCZN/Li cells under different external voltages and temperatures are shown in Fig. S5a–d.† It can be observed that the total impedance (R_{total}) also decreases with higher external voltage. Assuming that R_{total} consists of electronic impedance (R_e) and ionic impedance (R_{Li^+}), which are connected in parallel, R_{total} can then be expressed using the following equation:

$$1/R_{total} = 1/R_e + 1/R_{Li^+} \quad (2)$$

Since the applied voltage has very little impact on R_{Li^+} (shown in Fig. S6†), its value can be considered as a constant. Therefore, different values of R_e can be calculated by simple math (shown in Fig. S5e–h†). Then, the electronic current can be calculated according to the Ohm's law as shown in Fig. 3, where all curves also exhibit potential barrier breakdown behavior. The values of V_T under this circumstance (V_T') are listed in Table 1. It is found that the values of V_T' match exceptionally well with V_{sc} values obtained at the same temperatures, indicating a strong correlation between V_T' and the short circuit of LLCZN: during galvanostatic cycling, if the voltage polarization caused by ion conduction exceeds the critical point (*i.e.* V_T'), the grain boundary will become highly electron conductive. As a result, Li-ions will quickly combine with electrons, forming metallic Li that results in the short-circuit of the solid electrolyte.[15]

Table 1 Values of V_{sc} and V_T obtained at different temperatures

T (°C)	25	40	50	60
V_{sc}	0.261	0.195	0.163	0.125
V_T'	0.270	0.186	0.153	0.108

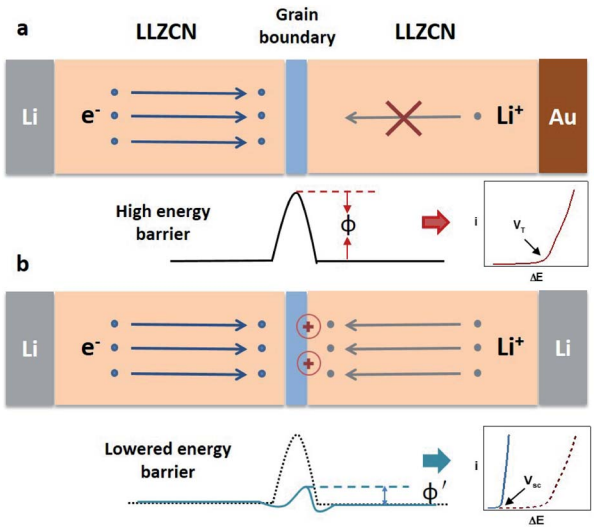

Scheme 1 Schematic illustration of different electron-transfer energy barriers at the grain boundary of LLCZN in the (a) Au/LLCZN/Li cell and (b) Li/LLCZN/Li cell.

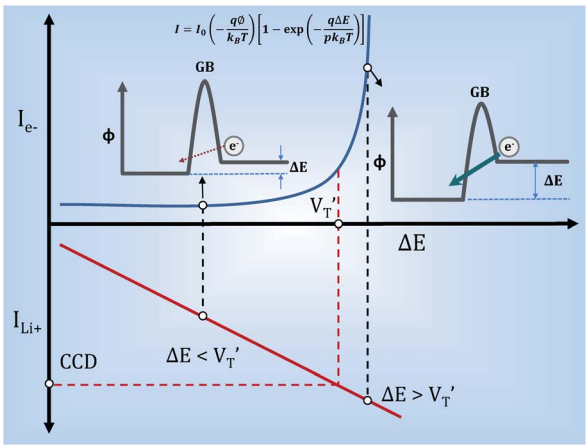

Scheme 2 Proposed scheme of electron conduction at grain boundaries under different external potentials.

The proposed schemes of electron conduction mechanisms are demonstrated in Scheme 1. On the one hand, as shown in Scheme 1a, because electrons are the only charge carriers in Au/LLCZN/Li cells when a positive external voltage is applied on the Au electrode, the electron-transfer energy barriers at grain boundaries are relatively high. As a result, a high external voltage is necessary to overcome E_{GB}, hence a much higher V_T is obtained. On the other hand, in Scheme 1b, by replacing the Au electrode with Li^0, Li-ions become the main charge carriers in Li/LLCZN/Li cells. Therefore, by applying a relatively small voltage, one side of the grain boundary will be concentrated with Li^+. This assumption is supported by the slow decay of the residual polarization of the Li/LLCZN/Li cell after applying an external voltage of 0.2 V shown in Fig. S7.† The positively charged grain boundary forms an electric field which attracts electrons from the other side and therefore lowers E_{GB}. Consequently, instead of a high V_T, a much lower V_{sc} (V_T') is obtained for Li/LLCZN/Li.

Conclusions

In this work, a new model of electron conduction that leads to the short circuit of garnet-type SSEs is proposed as shown in Scheme 2. It is revealed that in the presence of an external electric field (ΔE) that exceeds a threshold voltage (V_T), the solid electrolyte will undergo an electric breakdown process by exhibiting an electronic conductivity surge. Consequently, massive amounts of electrons will combine with Li-ions at grain boundaries eventually leading to a short circuit. Therefore, in order to effectively avoid the short circuit, it is necessary to keep $\Delta E < V_T$. To achieve this goal, methods for either reducing the voltage polarization (*e.g.* improving ionic conductivity and facilitating a well contacted interface) or increasing the energy barrier of electron transfer at grain boundaries (*e.g.* a thin coating on SSE particles or doping in SSEs) are expected to be particularly effective.

Conflicts of interest

There are no conflicts to declare.

Acknowledgements

Y. S. and L. Y. contributed equally to this work. This work was supported by the National Key R&D Program of China (2016YFB0700600) and Soft Science Research Project of Guangdong Province (2017B030301013).

Notes and references

1 J. Xiang, L. Yang, L. Yuan, K. Yuan, Y. Zhang, Y. Huang, J. Lin, F. Pan and Y. Huang, *Joule*, 2019, DOI: 10.1016/j.joule.2019.07.027.
2 E. J. Cheng, A. Sharafi and J. Sakamoto, *Electrochim. Acta*, 2016, **223**, 85–91.
3 F. Shen, M. B. Dixit, X. Xiao and K. B. Hatzell, *ACS Energy Lett.*, 2018, **3**, 1056–1061.
4 C. V. Chandran, C.-L. Tsai, V. Roddatis, P. Heitjans, M. Bram, S. Uhlenbruck, O. Guillon and Q. Ma, *ACS Appl. Mater. Interfaces*, 2016, **8**, 10617–10626.
5 Y. Takeda, H. Nemori, N. Imanishi, R. Sudo, S. Sunahiro, M. Matsui, Y. Nakata, O. Yamamoto and K. Ishiguro, *J. Electrochem. Soc.*, 2014, **161**, A668–A674.
6 R. Sudo, Y. Nakata, K. Ishiguro, M. Matsui, A. Hirano, Y. Takeda, O. Yamamoto and N. Imanishi, *Solid State Ionics*, 2014, **262**, 151–154.
7 T. Swamy, B. W. Sheldon, S. Berendts, H. L. Thaman, D. Rettenwander, L. Porz, W. C. Carter, R. Uecker, Y.-M. Chiang and T. Frömling, *Adv. Energy Mater.*, 2017, **7**, 1701003.
8 A. Sharafi, E. Kazyak, A. L. Davis, S. Yu, T. Thompson, D. J. Siegel, N. P. Dasgupta and J. Sakamoto, *Chem. Mater.*, 2017, **29**, 7961–7968.
9 H. M. Meyer, J. Nanda, J. Wolfenstine, J. Sakamoto and A. Sharafi, *J. Power Sources*, 2015, **302**, 135–139.
10 H. Buschmann, J. Dölle, S. Berendts, A. Kuhn, P. Bottke, M. Wilkening, P. Heitjans, A. Senyshyn, H. Ehrenberg, A. Lotnyk, V. Duppel, L. Kienle and J. Janek, *Phys. Chem. Chem. Phys.*, 2011, **13**, 19378.
11 J. F. Wu, B. W. Pu, D. Wang, S. Q. Shi, N. Zhao, X. Guo and X. Guo, *ACS Appl. Mater. Interfaces*, 2019, **11**, 898–905.
12 F. Han, A. S. Westover, J. Yue, X. Fan, F. Wang, M. Chi, D. N. Leonard, N. J. Dudney, H. Wang and C. Wang, *Nat. Energy*, 2019, **4**, 187–196.
13 H. K. Tian, B. Xu and Y. Qi, *J. Power Sources*, 2018, **392**, 79–86.
14 F. Aguesse, W. Manalastas, L. Buannic, J. M. L. Del Amo, G. Singh, A. Llordés and J. Kilner, *ACS Appl. Mater. Interfaces*, 2017, **9**, 3808–3816.
15 Y. Song, L. Yang, W. Zhao, Z. Wang, Y. Zhao, Z. Wang, Q. Zhao, H. Liu and F. Pan, *Adv. Energy Mater.*, 2019, 1900671.
16 X. Han, Y. Gong, K. Fu, X. He, G. T. Hitz, J. Dai, A. Pearse, B. Liu, H. Wang, G. Rubloff, Y. Mo, V. Thangadurai, E. D. Wachsman and L. Hu, *Nat. Mater.*, 2017, **16**, 572–579.
17 L. Fan, S. Wei, S. Li, Q. Li and Y. Lu, *Adv. Energy Mater.*, 2018, **8**, 1702657.
18 H. Buschmann, S. Berendts, B. Mogwitz and J. Janek, *J. Power Sources*, 2012, **206**, 236–244.

19 P. R. Bueno, J. A. Varela and E. Longo, *J. Eur. Ceram. Soc.*, 2008, **28**, 505–529.
20 J. Li, Z. Xu, F. Li, X. Zhu and S. Zhang, *RSC Adv.*, 2016, **6**, 20074–20080.
21 J. Zhao, B. Wang and K. Lu, *Ceram. Int.*, 2014, **40**, 14229–14234.
22 J. Li, S. Li, F. Liu, M. A. Alim and G. Chen, *J. Mater. Sci.: Mater. Electron.*, 2003, **14**, 483–486.
23 X. Li, L. Xu, L. Liu, Y. Wang, X. Cao, Y. Huang, C. Meng and Z. Wang, *J. Mater. Chem. A*, 2014, **2**, 16740–16745.
24 D. C. Sinclair, T. B. Adams, F. D. Morrison and A. R. West, *Appl. Phys. Lett.*, 2002, **80**, 2153–2155.